RSC Advances

This article can be cited before page numbers have been issued, to do this please use: R. Mannam, B. Francis, S. K. Eswaran, N. Dasgupta and M.S. R. Rao, *RSC Adv.*, 2016, DOI: 10.1039/C6RA21529G.

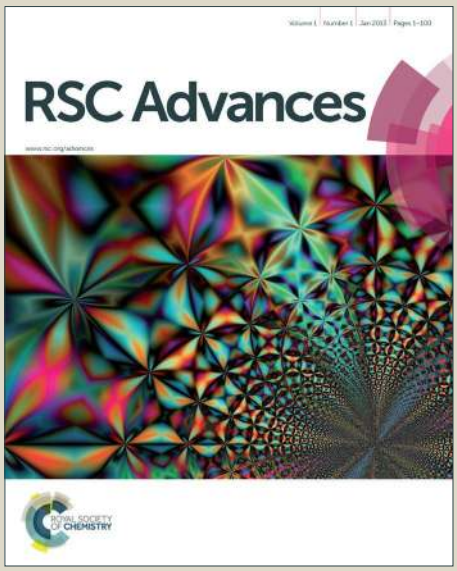

ROYAL SOCIETY OF CHEMISTRY

www.rsc.org/advances

View Article Online
DOI: 10.1039/C6RA21529G

RSC Advances

COMMUNICATION

Polarity control and enhanced luminescence characteristics of semi-polar ZnO nanostructures grown on non-polar MgO (100) substrates†

Received 00th January 20xx,
Accepted 00th January 20xx

DOI: 10.1039/x0xx00000x

www.rsc.org/

Ramanjaneyulu Mannam[a*] F. Bellarmine[a], E. Senthil Kumar[b] Nandita DasGupta[c] and M. S. Ramachandra Rao[a*]

Enhancing luminescence characteristics is one of the key challenges in ZnO nanostructures for highly efficient UV-blue LEDs and laser diodes. Non-conventional PLD growth parameters have been used to tailor the polar and semi-polar surfaces of ZnO nanostructures on MgO substrates. Despite the similar growth temperature, use of N_2 ambient gas allowed to fabricate well-aligned polar nanostructures; whereas, nanostructures grown with Ar ambient are semi-polar in nature. By means of cathodoluminescence spectroscopy, we demonstrate that the UV emission can be significantly enhanced by 11 times for semi-polar nanostructures. The enhanced luminescence is attributed to reduced polarization electric fields along c-axis.

ZnO is a brilliant UV emitter with wide and direct bandgap (~ 3.35 eV) and substantially large free exciton binding energy (~ 60 meV) at room temperature.[1] Despite the tremendous advancements in growth of epitaxial ZnO layers, considerable efforts on design and fabrication of ZnO nanostructures have been continuously made for widespread applications.[2-4] In particular, growth of non-polar ZnO nanostructures has been of great interest for the possibility of fabricating high efficiency UV emitters.[5] Absence of polarization electric fields in the non-polar nanostructures opens up the possibility of reducing the so-called quantum confined stark effect that ultimately enhances the luminescence characteristics.[6-8] Hence, the key to enhance the rate of probability of radiative recombination to realize intense UV emission is to successfully grow the non-polar or semi-polar ZnO nanostructures.[9]

The interest in control of polar and non-polar surfaces has driven the study of ZnO growth on various substrates. For example, c-axis oriented polar ZnO can be readily grown on sapphire (0001) and GaN substrates; whereas, cubic MgO substrates can lead to both polar and non-polar ZnO depending on the growth conditions.[10, 11] Use of MgO buffer layer on sapphire substrates also has greatly affected the polarity of ZnO layers.[12] Moreover, integrating wurtzite ZnO on cubic MgO is intriguing for many future applications such as, heterostructures for two dimensional electron gas, tunnel junctions and optoelectronic devices[13-16] Notwithstanding the promising results of ZnO in nanostructured form, earlier reports on tailoring the polarity of surfaces has mainly focused on the epitaxial thin films.[11] There have been many reports on the growth of ZnO thin films on MgO substrates with polar and non-polar surfaces.[11, 17-20] In contrast, only limited reports are available on the growth of ZnO nanostructures on MgO substrates.[18, 21] We have not found any report on the control of polar and non-polar surfaces of ZnO nanostructures on MgO substrates using carrier gas ambient.

In this work, for the first time, we present the control of polar and semi-polar ZnO nanostructures on MgO (100) substrates using pulsed laser deposition (PLD) with non-conventional growth parameters. Despite the similar growth temperatures, use of N_2 ambient gas resulted in ZnO nanostructures with polar surfaces; whereas use of Ar-gas led to the growth of semi-polar surfaces. Use of N_2 gas promotes aligned one-dimensional nanorods, which are perpendicular to MgO (100) surface. We show a similar effect even for phosphorous-doped ZnO nanostructures. Nanostructures grown under N_2 ambient exhibited an additional Raman mode at 277 cm^{-1}, which is characteristic of nitrogen-induced Zn interstitial clusters[22]. We demonstrate by means of cathodoluminescence (CL) spectroscopy that the as-grown semi-polar nanostructures show enhanced luminescence with integrated intensity of UV emission 11 times larger than that observed from polar surfaces. The enhanced CL emission is attributed to the reduction in polarization electric fields along the semi-polar surfaces. Our findings suggest that different crystallographic orientations of the ZnO nanostructures can be utilized as independent degrees of freedom to control the UV emission characteristics of optoelectronic devices.

[a] Department of Physics, Nano Functional Materials Technology Centre and Materials Science Research Centre, Indian Institute of Technology Madras, Chennai-600036, India. Email: msrrao@iitm.ac.in & ramu.nov9@gmail.com
[b] SRM Research Institute, Department of Physics and Nanotechnology, SRM University, kattankulathur – 603203, Tamil Nadu, India
[c] Microelectronics and MEMS Laboratory, Electrical Engineering Department, Indian Institute of Technology Madras, Chennai-600036, India
†Electronic Supplementary Information (ESI) available. See DOI: 10.1039/x0xx00000x

View Article Online
DOI: 10.1039/C6RA21529G

Non-catalyst assisted ZnO nanostructures growth on MgO (100) substrates was carried out using PLD technique at an optimized substrate-temperature of 800 ^{o}C. A KrF excimer laser was used for the growth of nanostructures with a repetition rate of 10 Hz and an energy density of 2.7 Jcm^{-2}. Either Ar or N_2 were used as ambient gas with a flow of 100 sccm (standard cubic centimeters per minute) that keeps the chamber pressure during the growth at 5 mbar. It is worth noting that the growth pressure used here is few orders of magnitude larger than that used for typical thin films fabrication. The growth was carried out for 15 min. Similar growth conditions were used for fabricating P doped (1 mol %) ZnO nanostructures. The microstructure analysis was carried out using field emission scanning electron microscopy (FESEM, FEI, Inspect F). Structural properties were investigated via X-ray diffraction (XRD) using Rigaku multipurpose XRD unit in ω-2θ and Φ-scan mode. Raman Spectra were collected in backscattering geometry with 488 nm of Ar^{+} laser using HORIBA Jobin Yuvon spectrometer. XPS measurements were performed using SPECS with PHIBOS100 energy analyser (SPECS GmbH, Germany), Al (Kα: 1486.61 eV) radiation was used to excite the electrons. The CL spectroscopy was carried out with Gatan CL system equipped on a Zeiss SEM.

Fig. 1a and b shows a comparison of FESEM images of undoped ZnO nanostructures grown under identical conditions but with differ ambient gas. Use of different ambient gas resulted in a dramatic change in morphology of the nanostructures. As shown in Fig. 1a, the nanorods grown under N_2 ambient are well aligned to each other and perpendicular to the substrate with their (000*l*) face parallel to the substrate surface. On the other hand, use of Ar gas resulted in nanorods with tapering at the tip as shown in Fig. 1b. Even though the nanorods are perpendicular to the substrate, other facets like {10-11} are also observed with clear hexagonal six-fold symmetry. This reveals that the semi-polar ZnO nanostructures can be fabricated with Ar as ambient gas,

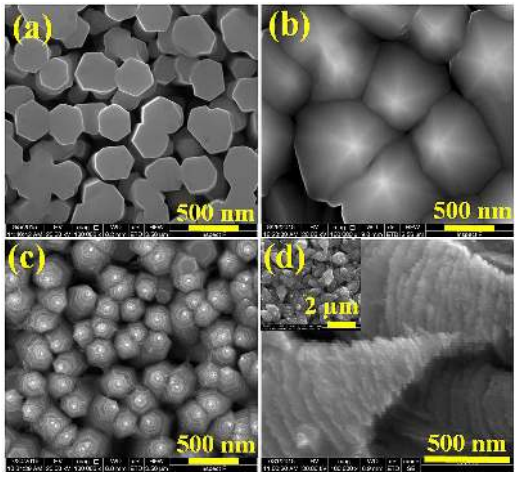

Fig. 1 Top view of FESEM images of (a) undoped ZnO nanostructures grown under N_2. (b) undoped ZnO nanostructures grown under Ar gas. (c) P doped ZnO structures grown under N_2. (d) P doped ZnO structures grown under Ar. Inset of figure (d) shows random alignment

whereas the use of N_2 results in polar surfaces. It is well known that doping has a strong influence on the morphology of the ZnO nanostructures. To understand the combined effect of ambient gas and doping on the polarity control of the ZnO nanostructures, we have fabricated P doped ZnO nanostructures under similar growth conditions of undoped nanostructures. P doped ZnO nanostructures exhibited cone like morphology as shown in micrographs in Fig. 1c and 1d correspond to nanostructures grown under N_2 and Ar ambient gases respectively. Nevertheless, the tendency to switch from polar to semi-polar surfaces when changing the ambient gas from N_2 to Ar is persistent even for P doped ZnO nanostructures. This clearly reveals that, regardless of doping, the key processing parameter to control the crystallographic orientation of the ZnO nanostructures is the ambient gas. During the ablation of ZnO target at the growth temperature of 800 ^{o}C, initially the ablated Zn atoms forms a liquid droplet and acts as self-catalyst for further nanostructures growth. This Zn liquid droplet precipitates and oxidize to form ZnO as the time progress. Since the gas ambiets in our case are Ar and N_2, the only source of O is the ZnO target used for ablation. For the nanostructures grown in Ar ambient, most of the 'O' from ZnO target is utilized to oxidize the Zn that leads to higher growth rate at sides, steps and terraces.[23] This results in expanded 2D growth and hence semi-polar nanocones are favoured. On the other hand, when using N_2 ambient, there is a possibility that a fraction of the oxygen is utilized to form oxynitrates (NOx). Hence the relatively less availability of oxygen reduces the growth rate at the nanorod sides and steps leading to a well-aligned c-axis oriented polar nanorods[23].

To further understand the crystallographic orientations of the as-grown ZnO nanostructures, we have performed detailed XRD measurements. The ω-2θ scans of undoped and P doped nanostructures grown under N_2 ambient suggests that the nanorods are predominantly oriented along the polar c-axis (000*l*) of the wurtzite hexagonal structure (Fig. 2a). The XRD patterns are consistent with the SEM micrographs. In addition to reflection corresponding to polar (0002) plane, the undoped and P doped nanostructures grown under Ar ambient exhibited (100) and (10-11) reflections in the XRD pattern

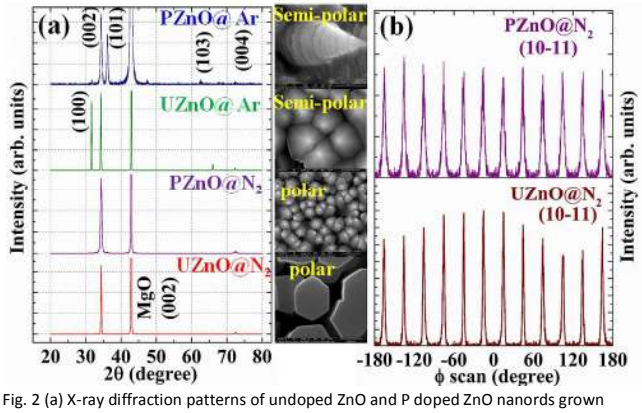

Fig. 2 (a) X-ray diffraction patterns of undoped ZnO and P doped ZnO nanords grown under both N_2 gas and Ar gas ambients respectively. (b). X-ray phi-scans of undoped and P doped ZnO nanostructures grown under N_2 respectively.

View Article Online
DOI: 10.1039/C6RA21529G

revealing the semi-polar nature of the growth. Epitaxial nature of the ZnO nanostructures grown under N_2 ambient was investigated with XRD Φ-scans. The typical Φ-scan of the (10-11) ZnO plane of the undoped and P doped nanostructures are given in Fig. 2b. The appearance of the twelve equidistance peaks separated by 30° suggests that the nanostructures have two different domains, which are rotated by 30° with respect to each other.

Fig. 3a and b show the Raman spectra of undoped and P doped ZnO nanostructures grown under Ar as ambient gas. The Raman spectra is dominated by the peaks at 98.1, 439.9 and 586 cm^{-1} corresponding to E_2 (Low), E_2 (high) and E_1 (LO) modes of the wurtzite hexagonal ZnO with C_{6v} symmetry. The E_1 (LO) mode is attributed to the presence of defects such as oxygen vacancies, zinc interstitials and free carriers or defect complexes. Interestingly, as shown in Fig. 3c and d, both the undoped and P doped nanostructures grown under N_2 ambient exhibited additional Raman modes at 276, 510 and 582 cm^{-1}, which are generally forbidden modes. Earlier, the mode at 276 cm^{-1} was believed to be fingerprint for N doped ZnO and assigned as local vibrational mode (LVM) of N in ZnO lattice.[24] Observation of the same mode with other dopants indicates that 276 cm^{-1} might be a dopant induced defect mode.[25] Recently, Gluba *et al.*,[26] have convincingly showed

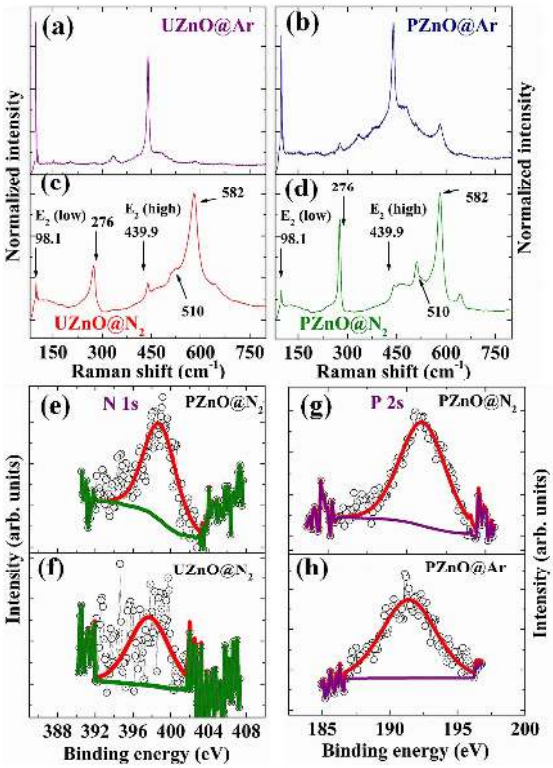

Fig. 3 Raman spectra of (a) undoped ZnO nanostructures grown under Ar. (b) P doped ZnO nanostructures grown under Ar gas. (c) undoped ZnO nanostructures grown under N_2. (d) P doped ZnO nanostructures grown under N_2 respectively. (e) and (f) XPS spectra of N 1s region of undoped and P doped ZnO nanostructures grown under N_2 gas respectively. (g) and (h) XPS spectra of P 2s region of P doped ZnO nanostructures grown under both N_2 and Ar gas atmospheres respectively

that the mode at 276 cm^{-1} is associated with interstitial zinc clusters. Hence it can be understood that during the growth of nanostructures under N_2 ambient there is a possibility of N doping in ZnO lattice that induces the Zn interstitials (Zn_i).

In order to test the possibility of N doping in ZnO lattice, we have carried out XPS measurements for the undoped and P doped nanostructures grown under N_2 ambient. As shown in Fig. 3e and f, XPS spectra of both the P doped and undoped nanostructures exhibited a peak around 397 eV, which is Well-known to be associated with 1*s* level of N substituted at O site in ZnO thin films.[27] This clearly confirms the doping of N during ZnO nanostructures growth utilizing N_2 ambient as nitrogen source. This is in very good agreement with the Raman spectra, which shows the evidence of N substitution in ZnO nanostructures grown under N_2 ambient. Fig. 3g and h shows the P 2*s* level of P doped samples grown under both N_2 and Ar ambient. The peak around 191.4 eV corresponds to P^{5+} state. We did not observe any peak around 186 eV, which is associated with P^{3-} state.[28] Hence our observations suggest that P is substituted at Zn site in P^{5+} state rather than at the oxygen site.[29, 30]

Fig. 4a shows the room temperature CL spectra of undoped ZnO nanostructures, grown under both Ar and N_2 ambient, collected with an irradiation of 15 kV electron beam on the samples at 50000 x magnification. The CL spectra consisted of typical UV emission around 386 nm, which is ascribed to near-band-edge (NBE) emission, and the mid-band gap related visible luminescence due to various point defects. The visible green luminescence of the semi-polar nanostructures is located around ~ 550 nm (Fig. S1 in ESI†) that is recently found to be originated from defects at the (10-10) surfaces.[31] On the other hand polar nanostructures exhibited visible luminescence bands at 409 nm and 465 nm (Fig. S2†). The peak at 409 nm is associated with electronic transition from

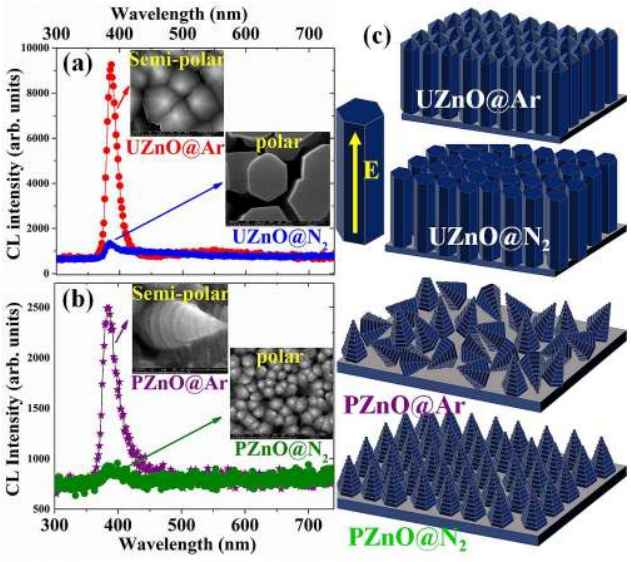

Fig. 4 CL spectra of (a) undoped ZnO nanostructures grown under Ar and N_2 ambient respectively. (b) P doped ZnO nanostructures grown under Ar and N_2 ambient respectively and (c) Schematics of undoped and P doped ZnO nanostructures grown in both polar and semi-polar directions.

View Article Online
DOI: 10.1039/C6RA21529G

conduction band to zinc vacancies (V_{Zn}); whereas, the peak at 465 nm is due to the transition from Zn_i to V_{Zn}.[29] This is a further confirmation for the N induced formation of Zn_i and V_{Zn} in polar nanostructures. It is noteworthy that the integrated CL intensity of the semi-polar ZnO nanostructures is 11 times larger than that of the polar nanostructures. Similarly for P doped samples the ratio of the integrated CL intensity of semi-polar to polar nanostructures is 17. When comparing the CL emission intensities of semi-polar nanostructures, the undoped nanostructures exhibit 3 times stronger emission than P doped samples. Several other groups have also reported enhanced luminescence characteristics for non-polar epitaxial layers in the past.[5, 7, 32]

The enhanced CL emission of the semi-polar ZnO nanostructures can be qualitatively understood from the relationship between the orientation of different crystallographic surfaces and polarization electric field. As shown in Figure 4c that for well aligned polar ZnO nanorods (undoped) and nanocones (P doped), the spontaneous polarization along the c-axis due to lack of inversion symmetry results a large net electric field perpendicular to the substrate. During CL measurement, when an electron beam hits the polar ZnO nanostructures, an electron-hole pair (exciton) is created. However the presence of large internal electric field decreases the overlapping of the electron and hole wave functions and consequently decreases the probability of radiative recombination. On the other hand for semi-polar nanostructures, the internal polarization field is greatly minimized and hence a strong overlapping of electron-hole pair occurs that enhances the radiative recombination. This is the reason why the semi-polar ZnO nanostructures exhibited strong CL emission intensity when compared with that of polar nanostructures.

In conclusion, we have successfully demonstrated the controlled fabrication of polar and semi-polar ZnO nanostructures on MgO substrates using pulsed laser deposition by carefully selecting suitable ambient gas conditions. With the P doping as an example case, we showed the similar results of polarity control even for doped samples. CL spectroscopy results indicate the enhancement in UV emission intensity of semi-polar nanostructures. As a significant indicator, the integrated CL intensities of semi-polar nanostructures are as large as 11 times that observed from polar nanostructures. The reduced polarization electric field in the semi-polar nanostructures resulted the enhanced luminescence characteristics. These results are indeed encouraging from the view point of utilizing the semi-polar nanostructures for better light emission in LEDs and laser diodes.

Acknowledgment

The authors thank Department of Science and Technology (DST), New Delhi that facilitated the establishment of “Nano Functional Materials Technology Centre” (Grant: SRNM/NAT/02-2005).

Notes and references

1. Ü. Özgür, Y. I. Alivov, C. Liu, A. Teke, M. A. Reshchikov, S. Doğan, V. Avrutin, S.-J. Cho and H. Morkoç, *J. Appl. Phys.*, 2005, **98**, 041301.
2. C. Li, C. Li, Y. Di, W. Lei, J. Chen and Y. Cui, *ACS Appl. Mater. Interfaces*, 2013, **5**, 9194-9198.
3. W. Y. Weng, S. J. Chang, C. L. Hsu and T. J. Hsueh, *ACS Appl. Mater. Interfaces*, 2011, **3**, 162-166.
4. X. Tang, G. Li and S. Zhou, *Nano Lett.*, 2013, **13**, 5046-5050.
5. S. Chen, X. Pan, H. He, W. Chen, J. Huang, B. Lu and Z. Ye, *Opt. Lett.*, 2015, **40**, 3639-3642.
6. P. Waltereit, O. Brandt, A. Trampert, H. T. Grahn, J. Menniger, M. Ramsteiner, M. Reiche and K. H. Ploog, *Nature*, 2000, **406**, 865-868.
7. M. Leroux, N. Grandjean, M. Laügt, J. Massies, B. Gil, P. Lefebvre and P. Bigenwald, *Phys. Rev. B*, 1998, **58**, R13371-R13374.
8. C. Morhain, T. Bretagnon, P. Lefebvre, X. Tang, P. Valvin, T. Guillet, B. Gil, T. Taliercio, M. Teisseire-Doninelli, B. Vinter and C. Deparis, *Phys. Rev. B*, 2005, **72**, 241305.
9. J.-J. Chen, X.-R. Deng and H. Deng, *J. Mater. Sci*, 2013, **48**, 532-542.
10. S.-B. Mi, *Thin Solid Films*, 2014, **558**, 237-240.
11. S. H. Seo and H. C. Kang, *J. Cryst. Growth*, 2011, **326**, 166-170.
12. H. Kato, K. Miyamoto, M. Sano and T. Yao, *Appl. Phys. Lett.*, 2004, **84**, 4562-4564.
13. A. Tsukazaki, A. Ohtomo, T. Kita, Y. Ohno, H. Ohno and M. Kawasaki, *Science*, 2007, **315**, 1388-1391.
14. D. L. Li, Q. L. Ma, S. G. Wang, R. C. C. Ward, T. Hesjedal, X. G. Zhang, A. Kohn, E. Amsellem, G. Yang, J. L. Liu, J. Jiang, H. X. Wei and X. F. Han, *Sci. Rep.*, 2014, **4**, 7277.
15. H. Zhou, H.-Q. Wang, L. Wu, L. Zhang, K. Kisslinger, Y. Zhu, X. Chen, H. Zhan and J. Kang, *Appl. Phys. Lett.*, 2011, **99**, 141917.
16. H. Zhou, H.-Q. Wang, Y. Li, K. Li, J. Kang, J.-C. Zheng, Z. Jiang, Y. Huang, L. Wu, L. Zhang, K. Kisslinger and Y. Zhu, *ACS Appl. Mater. Interfaces*, 2014, **6**, 13823-13832.
17. C. Y. J. Lu, L. Chang, K. H. Ploog and M. M. C. Chou, *J. Cryst. Growth*, 2013, **378**, 172-176.
18. R. Deng, B. Yao, Y. F. Li, B. H. Li, Z. Z. Zhang, H. F. Zhao, J. Y. Zhang, D. X. Zhao, D. Z. Shen, X. W. Fan, L. L. Yang and Q. X. Zhao, *J. Cryst. Growth*, 2009, **311**, 4398-4401.
19. L. C. Nistor, C. Ghica, D. Matei, G. Dinescu, M. Dinescu and G. Van Tendeloo, *J. Cryst. Growth*, 2005, **277**, 26-31.
20. N. Matsunami, M. Itoh, Y. Takai, M. Tazawa and M. Sataka, *Nuclear Instruments and Methods in Physics Research Section B: Beam Interactions with Materials and Atoms*, 2003, **206**, 282-286.
21. J. H. He, C. H. Ho, C. W. Wang, Y. Ding, L. J. Chen and Z. L. Wang, *Cryst. Growth Des.*, 2009, **9**, 17-19.
22. P. Zhang, C. Kong, W. Li, G. Qin, Q. Xu, H. Zhang, H. Ruan, Y. Cui and L. Fang, *Appl. Surf. Sci.*, 2015, **327**, 154-158.
23. S. Li, X. Zhang and L. Zhang, *The J.Phys. Chem C*, 2010, **114**, 10379-10385.
24. J. Yu, H. Xing, Q. Zhao, H. Mao, Y. Shen, J. Wang, Z. Lai and Z. Zhu, *Solid State Commun*, 2006, **138**, 502-504.

View Article Online
DOI: 10.1039/C6RA21529G

25. Q. Cao, M. Fu, G. Liu, H. Zhang, S. Yan, Y. Chen, L. Mei and J. Jiao, *J. Appl. Phys.*, 2014, **115**, 243906.
26. M. A. Gluba, N. H. Nickel and N. Karpensky, *Phys. Rev. B*, 2013, **88**, 245201.
27. D. Zhang, J. Gong, J. Ma, G. Han and Z. Tong, *Dalton Trans.*, 2013, **42**, 16556-16561.
28. Y. W. Heo, K. Ip, S. J. Park, S. J. Pearton and D. P. Norton, *Appl. Phys. A*, 2004, **78**, 53-57.
29. R. Mannam, S. K. Eswaran, N. DasGupta and M. S. R. Rao, *Appl. Surf. Sci.*, 2015, **347**, 96-100.
30. L. Guan, B. Liu, Q. Li, Y. Zhou, J. Guo, G. Jia, Q. Zhao, Y. Wang and G. Fu, *Phys. Lett. A*, 2011, **375**, 939-945.
31. F. Fabbri, M. Villani, A. Catellani, A. Calzolari, G. Cicero, D. Calestani, G. Calestani, A. Zappettini, B. Dierre, T. Sekiguchi and G. Salviati, *Sci. Rep.*, 2014, **4**, 5158.
32. S. Chen, X. Pan, H. He, W. Chen, C. Chen, W. Dai, H. Zhang, P. Ding, J. Huang, B. Lu and Z. Ye, *Opt. Lett.*, 2015, **40**, 649-652.

View Article Online
DOI: 10.1039/C6RA21529G

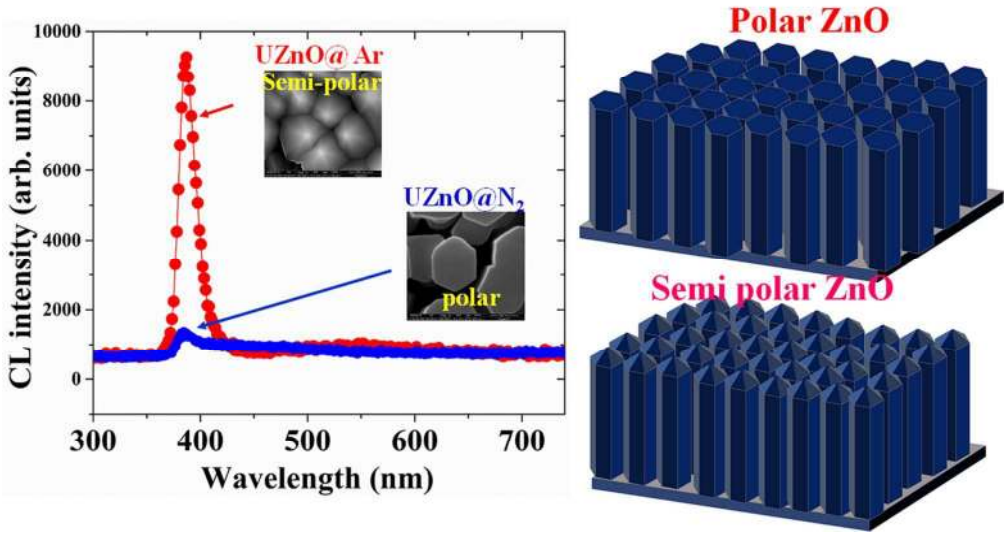

214x117mm (150 x 150 DPI)